NORDIC STEEL 2024
The 15th Nordic Steel Construction Conference,
June 26–28, 2024, Luleå, Sweden

Generic Substitute Imperfection Patterns for the GMNIA of Tanks and Silos made of Steel or Aluminium

Peter Knoedel*[,a], Tobias Wacker[b], Thomas Ummenhofer[c]

[a]Dr Knoedel Engineering Consultants, Baden-Baden, Germany
info@peterknoedel.de
[b]ANAKON GmbH, Karlsruhe, Germany
t.wacker@anakon.de
[c]KIT Steel and Lightweight Structrures, Karlsruhe Institute of Technology, Germany
thomas.ummenhofer@kit.edu

ABSTRACT

In EN 1993-1-6, several methods are offered for the stability design of shell structures. Most elaborate results are found by a GMNIA ("full analysis", EN 1993-1-6:2017 8.8) where geometric substitute imperfections and material non-linearities are accounted for in the numerical model. Typically, radial shape deviations are used, which represent a governing eigenmode, see EN 1993-1-6 8.8.2 (13) and (15). Rules for the maximum amplitude of the imperfection pattern are given in Tab. 8.5.

In practical design however, it is more convenient to use imperfection patterns, the shape of which is known a priori. E.g. Rotter/Teng (1989) presented an analytical description for an idealized circumferential weld depression, which has been proven to be sufficient for a realistic description of the resistance under axial compression. For other load cases and other manufacturing methods, such as joining the plates by bolted overlaps, these a priori imperfections have not been described so far.

In the present paper, a set of generic imperfection patterns for different load cases and different methods of manufacture is described by means of truncated double Fourier series. The patterns are investigated by exemplary GMNIA, so that the imperfection sensitivity of the different patterns can be demonstrated. Using this generic imperfection patterns, the structural engineer is able to script a universal imperfection generator. For each individual project, the Fourier coefficients of the relevant generic imperfection pattern are introduced. Thus, the aim of the paper is to simplify the handling of imperfection patterns with GMNIA.

Keywords: shell structures, stability, buckling, FE-modelling

1 INTRODUCTION

In this study we consider geometrical radial deviations from the perfect cylindrical shape as substitute imperfections. We investigate typical sets of these imperfection patterns and their impact on the capacity under specific load cases. The patterns are represented by truncated Fourier series, the amplitudes of which are determined e.g. from code provisions or from laser scan measurements.

The aim of this study is to provide easy-to-handle imperfection patterns to be used in GMNIA for practical design of tank and silo structures. Note that the authors recommended in a previous paper, not to use GMNIA in practical design (chap. 3 thesis 13 in (1)). However, there can be manifold reasons where GMNIA is still advantageous, e.g.

– Assessment of an existing tank, where imperfections have been measured, which are much in excess of the EC3-1-6 (2) provisions, see *Fig. 2*.
– Geometrical conditions, where EC3-1-6 (2) seems to predict unsatisfactory capacity, see hypothesis H13 in (3).

2 ABBREVIATIONS, TERMS AND DEFINITIONS

Note:	example sets of coefficient matrices can be downloaded from https://peterknoedel.de/search/search.htm
2D-(elliptical-)Bump – simplified Gauss Bell	$f_{i,j} = Amp \cdot e^{-\left(\frac{x_i - x_0}{\frac{d_x}{4}}\right)^2} \cdot e^{-\left(\frac{y_j - y_0}{\frac{d_y}{4}}\right)^2}$ (1) with Amp: depth; x_0; y_0 position of centre; d_x;d_y diameter
2D-DFT	DFT for a 2D surface, returns the Fourier coefficients to represent a 2D surface $A_{0,0} = \frac{1}{M} \cdot \frac{1}{N} \sum_{i=0}^{2M-1} \sum_{j=0}^{2N-1} w_{i,j}$ (2) $A_{m,n} = \frac{1}{M} \cdot \frac{1}{N} \sum_{i=0}^{2M-1} \sum_{j=0}^{2N-1} [w_{i,j} \cdot \cos(\frac{j \cdot n \cdot \pi}{N}) \cdot \cos(\frac{i \cdot m \cdot \pi}{M})]$ $B_{m,n} = \frac{1}{M} \cdot \frac{1}{N} \sum_{i=0}^{2M-1} \sum_{j=0}^{2N-1} [w_{i,j} \cdot \cos(\frac{j \cdot n \cdot \pi}{N}) \cdot \sin(\frac{i \cdot m \cdot \pi}{M})]$ $C_{m,n} = \frac{1}{M} \cdot \frac{1}{N} \sum_{i=0}^{2M-1} \sum_{j=0}^{2N-1} [w_{i,j} \cdot \sin(\frac{j \cdot n \cdot \pi}{N}) \cdot \cos(\frac{i \cdot m \cdot \pi}{M})]$ $D_{m,n} = \frac{1}{M} \cdot \frac{1}{N} \sum_{i=0}^{2M-1} \sum_{j=0}^{2N-1} [w_{i,j} \cdot \sin(\frac{j \cdot n \cdot \pi}{N}) \cdot \sin(\frac{i \cdot m \cdot \pi}{M})]$ The following statements are referring to the x- and y-direction respectively: $w_{i,j}$ = data points in the x (circumference) and y (meridian) direction; M,N = number of data pairs; i = 0 … 2M-1; j = 0 … 2N-1; counter of the data points; m = 1 … M; n = 1 … N; counter for the Fourier coefficients
D; L_{cyl}; $L_{strake,i}$; T_i; L_{dep};	dimensions of the cylindrical structure: diameter; total length bottom to eaves; length of strake; wall-thickness of strake; with i = counter of the strakes; meridional length of weld depression, see *Type A*
DBF	design by formulae (“hand calculation”) as opposite to e.g. numerical methods (EN 13445-3 5.4)
DFT	Discrete Fourier Transform; FT for discrete values – requires equidistant spacing of the data points; returns the Fourier coefficients to represent the data points $A_0 = \frac{1}{n} \sum_{j=0}^{2n-1} w_j$ $\quad A_k = \frac{1}{n} \sum_{j=0}^{2n-1} [w_j \cdot \cos(\frac{j \cdot k \cdot \pi}{n})]$ (3) $B_k = \frac{1}{n} \sum_{j=0}^{2n-1} [w_j \cdot sin(\frac{j \cdot k \cdot \pi}{n})]$ w_j = values in the time domain; n = number of data pairs; j = 0 … 2n-1 counter for the values; k = 1 … n index of the Fourier coefficients
Double Fourier series, for coefficients see Eq. (3)	(truncated) Fourier series for a translatory 2D surface $S_{i,j} = \frac{A_{1,1}}{2} + \sum_{m=1}^{M} \sum_{n=1}^{N} [\cos(\frac{m \cdot x_i \cdot 2\pi}{L_{strake}}) \cdot A_{m,n} \cos((n-1) \cdot \theta_j)]$ (4)
Double Fourier series, for coefficients see Eq. (2)	(truncated) Fourier series for a general 2D surface $S_{A_{i,j}} = \frac{A_{0,0}}{2} + \sum_{m=1}^{M} \sum_{n=1}^{N} [A_{m,n} \cdot \cos(\frac{j \cdot n \cdot 2\pi}{T_y}) \cdot \cos(\frac{i \cdot m \cdot 2\pi}{T_x})]$ (5)

	$S_{B_{i,j}} = \sum_{m=1}^{M}\sum_{n=1}^{N}[B_{m,n} \cdot \cos(\frac{j \cdot n \cdot 2\pi}{T_y}) \cdot \sin(\frac{i \cdot m \cdot 2\pi}{T_x})]$ $S_{C_{i,j}} = \sum_{m=1}^{M}\sum_{n=1}^{N}[C_{m,n} \cdot \sin(\frac{j \cdot n \cdot 2\pi}{T_y}) \cdot \cos(\frac{i \cdot m \cdot 2\pi}{T_x})]$ $S_{D_{i,j}} = \sum_{m=1}^{M}\sum_{n=1}^{N}[D_{m,n} \cdot \sin(\frac{j \cdot n \cdot 2\pi}{T_y}) \cdot \sin(\frac{i \cdot m \cdot 2\pi}{T_x})]$ $S_{i,j} = S_{A_{i,j}} + S_{B_{i,j}} + S_{C_{i,j}} + S_{D_{i,j}}$
E; E_{pl}; ν; f_y	material parameters: Young's modulus 210 GPa; plastic modulus 210 MPa; Poisson's ratio 0,30; yield limit 235 MPa;
EC3	short form for EN 1993 (2)
Fourier series Fourier sum	(truncated) sum of harmonic functions with the Fourier coefficients A and B as amplitudes (4) $S_i = \frac{a_0}{2} + \sum_{j=1}^{k_{max}}[A_j \cdot \cos\left(k_j \cdot x_i \cdot \frac{2\pi}{L}\right) + B_j \cdot \sin\left(k_j \cdot x_i \cdot \frac{2\pi}{L}\right)]$ (6) $k = 0 \ldots k_{max}$; index for the Fourier coefficients; i = counter for the evaluated data points; j = counter for the k_{max} coefficients used;
FT	Fourier Transform; converts a function from the "time domain" into the "frequency domain"; thus, output of the FT are the coefficients of the Fourier series (4) $A_k = \frac{2}{T}\int_0^T f(x) \cdot \cos\,(k \cdot x \cdot \frac{2\pi}{T}) \cdot dx$ (7) $B_k = \frac{2}{T}\int_0^T f(x) \cdot \sin\,(k \cdot \mathrm{x} \cdot \frac{2\pi}{T}) \cdot dx$ $k = 0 \cdots \infty$; T = period of of the function
FTQC A, B, C (steel) Tol. class 4, 3, 2, 1 (alu)	fabrication tolerance quality classes, defined in EC3-1-6 8.4 (2); for aluminium, these are given in EN 1090-3:2019 H.2–H.4 (5)
GMNIA	geometrically and materially nonlinear analysis with imperfections explicitly included, term defined in EC3-1-6 1.3.5.10 (2)
Inverse FT Inverse DFT	Converting a function from the frequency domain (back) into the time domain; synonymous for Fourier series or double Fourier series
Weld depression Type A, B	Alternative meridional shapes of a circumferential weld depression according to (6) and (7) $w = w_0 \cdot e^{-\pi \cdot \frac{x}{\lambda}} \cdot [\cos\left(\frac{\pi \cdot x}{\lambda}\right) + \mathrm{k} \cdot \sin\left(\frac{\pi \cdot x}{\lambda}\right)]$ (8) with λ = 2,444 * √(R*T); k = 1 for Type A (tangent at the weld parallel to the meridian) and k = 0 for Type B (kink at the weld); note, that this formulation is only valid for x > 0; meridional size of depression (distance of zero crossings): L_{dep} = 3,666 * √(R*T) = 1,5 * λ

3 STATE-OF-THE-ART

3.1 Imperfections with meridionally compressed cylinders

An extensive discussion of imperfections is given in (8). Some of the content is repeated here with focus on describing and modelling imperfections for GMNIA.

It seems, that due to the dramatic reduction of capacity under meridional compression even with small imperfections, most of the research focused on this load case. Consequently, there is a vast number of scientific contributions on this matter, an overview can be found in (9).

In (10), a numerical elasto-plastic approach was used. The circumferential weld depression was based on measurements given in (11).
Teng and Rotter developed substitute weld depressions (6), (7) which are based on the theoretical bending shape of a meridian adjacent to an imposed radial displacement along a circumference.
(12) investigated the influence on random imperfections on the capacity of axially compressed cylinders. With localized imperfections far deeper than the limits of FTQC C, they achieved experimental buckling loads, the mean of which is 77 % above the prediction of EC3-1-6 (2); explanations are not given in the paper. Aluminium shells with random imperfections have been investigated in (13). However, the design rules derived for EC9-1-5 (14) seemed to have been faulty, which has been discussed in length in (15), (16).

3.2 Imperfections with radially compressed cylinders

The critical stresses are very low (app. 3 MPa for Tank B in chap. 4). After that, the loss due to imperfections is much smaller, compared to axially compressed cylinders. Furthermore, the buckling behaviour is “benign”: after bifurcation a stable postbuckling tensile membrane state develops, which allows for increasing loads associated with big radial displacements. Exemplary, the reader is referred to (17), where further references can be found.
Increasing use of cost-efficient laser survey of entire tank surfaces and subsequent GMNIA made evident, that a localized depression even with multiple depth of the codified limit imperfection does by far not have the influence on the capacity of the shell, that a more regular imperfection would have (see e.g. (18)). Thus, using eigenmode-imperfections with an amplitude taken from the respective FTQC, yields very conservative results.
There is another effect: the DBF designer ends up with a critical circumferential stress reduced by an empirical factor. The FEA designer approaches the bifurcation load asymptotically and then benefits from postbuckling membrane action. Thus, the former is designing very conservative against bifurcation, while the latter tackles a real 2nd or 3rd order ultimate load, see *Fig. 7 b)*.

3.3 Measuring and classifying imperfections

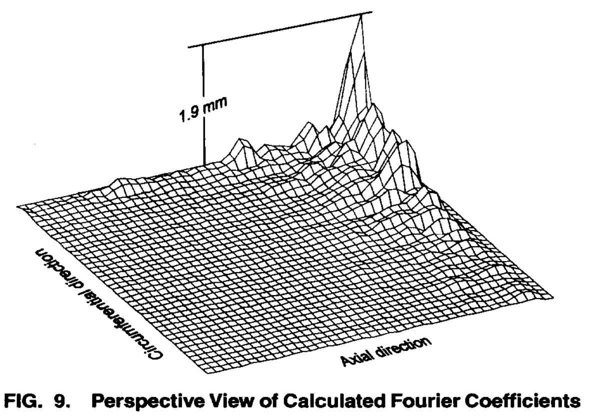

Fig. 1. Representation of the Fourier amplitudes (19)
41 coeff. in axial, 40 in circumf. direction;
big amplitues are grouped in the long-wave range

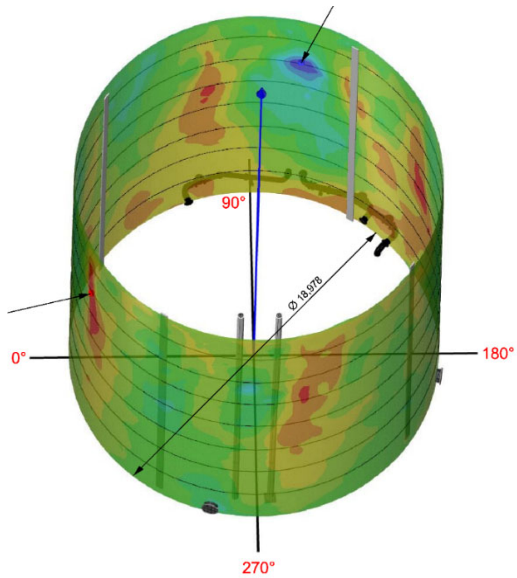

Fig. 2. Laser scan of an anonymized tank (page 19 in (20))
D = 19 m; H_{eaves} = 19 m; T_{act} ≈ 14; 12; 10; 8; 6; 5; 5; 5;
year built: app. 1969;
deviations from a perfect cylinder, $w_{extreme}$ ≈ +60/–95 mm;
yellow and redish is outward; green and blue is inward;

In (21) and (19) an accurate description is published on the measurement and evaluation techniques used on a 10.000 ton grain silo in Port Kembla, Wollongong, Australia. The radial deviations found were evaluated by means of a DFT, the amplitudes of which are shown in *Fig. 1*. These

measurements were re-evaluated by (22), including measurements of two other quasi-identical Port Kembla silos and focusing on different choices of Fourier series. It was found that the graphical representation of the Fourier coefficient matrices of the three different silos was very similar. Significant amplitudes are grouped along the first harmonics, and from the 20th harmonic onwards, the contributions may be neglected from an engineering point of view.
In (23), spiral welded tubes of app. 800 and 1.100 mm diameter were investigated. Double Fourier series were used to describe the surface imperfection pattern. In the next step, the mapping onto a FE grid was done by a Matlab command (23).
In engineering practice, laser survey of big structures such as tanks has become affordable routine. An example is shown in *Fig. 2*. Typically, with these tanks built in the 70s, imperfections are found, which are much in excess of the tolerances given in present design codes, e.g. EC3-1-6 8.4 (2). Dimple tolerances for exemplary structures are given in chap. 4.
In 1996, the authors published a typology of substitute imperfection patterns for the stability check of axially loaded cylinders (24). This study was extended in (8), when fabrication methods and load cases were considered additionally.

4 EXAMPLE STRUCTURES

Table 1. Dimple tolerance depth [mm] in FTQC A; B; C; acc. EC3-1-6:2017 8.4.4 (2) (steel) or Tolerance Class 3; 2; 1; acc. EN 1090-3:2019 H.2–H.4 (5) (aluminium)

Example structure	Meridional compression	Circumferential compression	Weld
Tank A; T_{eq} = 20 mm	14; 23; 37;	76; 127; 203;	3; 5; 8;
Tank B; T_{eq} = 10 mm	8; 13; 20;	17; 29; 46;	2; 3; 4;
Tank C; T = 5 mm	4; 6; 10;	17; 29; 46;	0,8; 1,3; 2,0;
Silo A; T_{eq} = 2,5 mm	1,2; 2,4; 4;	9; 15; 23;	0,4; 0,6; 1,0;
Silo B; T_{eq} = 4,5 mm	2; 3; 5;	9; 15; 24;	0,7; 1,1; 1,8;
Silo X; T = 3 mm	0,9; 1,5; 2,4;	3; 5; 8;	0,5; 0,8; 1,2;

In this study, we consider three tanks and three silos of typical size. From these we derive the range of parameters needed for the proposed method. All dimensions given are approximate.

TA: District heating tank Rostock, courtesy of IPU Karlsruhe (25)
D = 34.000 mm; L_{cyl} = 52.000 mm; L_{strake} = 2.900 mm; T = 11 mm – 38 mm
in this paper T_{eq} = 20 mm; L_{dep} = 2.138 mm

TB: Soyk/Knödel/Ponomarev (20) …
D = 20.000 mm; L_{cyl} = 20.000 mm; L_{strake} = 2.400 mm; T = 6 mm – 15 mm
in this paper T_{eq} = 10 mm; L_{strake} = 5.000 mm; L_{dep} = 1.159 mm

TC: Ummenhofer's and Knoedel's teaching tank (26)
D = 10.000 mm; L_{cyl} = 10.000 mm; L_{strake} = 2.000 mm; T = 5 mm; L_{dep} = 580 mm

SA: Carbon steel silo anonymous, courtesy of IPU, Karlsruhe
D = 2.900 mm; L_{cyl} = 14.000 mm; L_{strake} = 2.000 mm; T = 2 mm – 3 mm;
in this paper T_{eq} = 2,5 mm; L_{dep} = 221 mm

SB: Aluminium silo anonymous, given in (15)
D = 3.000 mm; L_{bin} = 10.000 mm; L_{strake} = 2.500 mm; T = 4 mm – 5 mm;
EN AW-5754 O/H111 (EN 485-2 (27)); in this paper T_{eq} = 4,5 mm; L_{dep} = 301 mm

SX: Silo model for structural tests "P3" (28), see also (29)
D = 900 mm; L_{cyl} = 1.000 mm (with stringers) + 1.250 mm; T = 3 mm
4 pairs of ribs at the local supports FL 25x8, e = 58 mm;
EN AW-5754 O/H111 (EN 485-2 (27)); coupon tests performed by KIT-VA showed mechanical properties corresponding to EN AW-5083 O/H111 (EN 485-2 (27))

5 GENERIC IMPERFECTION PATTERNS

5.1 Motivation

Most of the findings in chap. 3 are based on research projects, where measuring and evaluation of imperfections has been going on for months. This is not the time scale, in which the typical practitioner is trying to complete a re-evaluation of an existing tank. Therefore, we propose generic imperfection patterns, which are simplified and easy to use for the practitioner's GMNIA. Naturally, the accuracy of the calculations is reduced due to the simplification. However, it will be demonstrated, that the results are still within reasonable accuracy for practical design.

The advantage of using a Fourier representation is, that the imperfection surface itself is described to a desired accuracy. Based on this, the nodal initial radial position can be generated for any arbitrary mesh, independent of the mesh size or element shape. Thus, no restrictions appear during optimization of the mesh, convergence studies, etc.

5.2 Hypotheses and assumptions

H1 End rings and intermediate ring stiffeners provide sufficient radial stiffness to prevent significant radial deformations in a global buckling mode. Guidance for sufficient stiffness has been given in e.g. (17), see also EC3-4-2:2017 eq. 7.24 ff (30).

H2 It is sufficient to perform independent stability verifications of sub-divisions of the cylinder between end rings and/or intermediate stiffeners. Due to H1 global mode-shapes will not be governing. From H2 follows, that for each sub-division an individual generic imperfection pattern may be used.

H3 Amplitudes of the imperfection pattern, that amount to $\leq$ 10 % of the maximum amplitude, have no significant impact on the capacity of the shell, see *Fig. 6 b)*.

H4 One of the generic patterns describes equidistant circumferential welds. These need not coincide with the actual configuration, but provide comparable capacity as GMNIA result.

H5 The out of plane imperfections of a rolled and curved plate/panel prior to bolting or welding are assumed to be random. From an engineering point of view, this seems to be sufficient for the scope of the present study. From a scientific point of view, a more precise distinction can be made with respect to hot or cold rolling of the plate (see different levels of tolerances for structural steel hot rolled plates in EN 10029 Tab. 1 and structural steel cold rolled plates in EN 10143 Tab. 1), different materials (structural steel, stainless steel, aluminium) and cold or hot curving of the panel.

H6 Joining the strake's plates by bolted overlap does not induce significant imperfections. For DBF, reduction factors of 0,7 (meridional compression EC3-1-6 D.3.2 (1) (2); EC9-1-5 A.3.2 (1) (14)) and 0,9 (circumferential compression EC3-1-6 D.3.3 (1) (2); EC9-1-5 A.3.3 (1) (14)) are provided. In a GMNIA it is advantageous to model the actual offset of the mid-surfaces of the plates.

5.3 Curved panels without weld

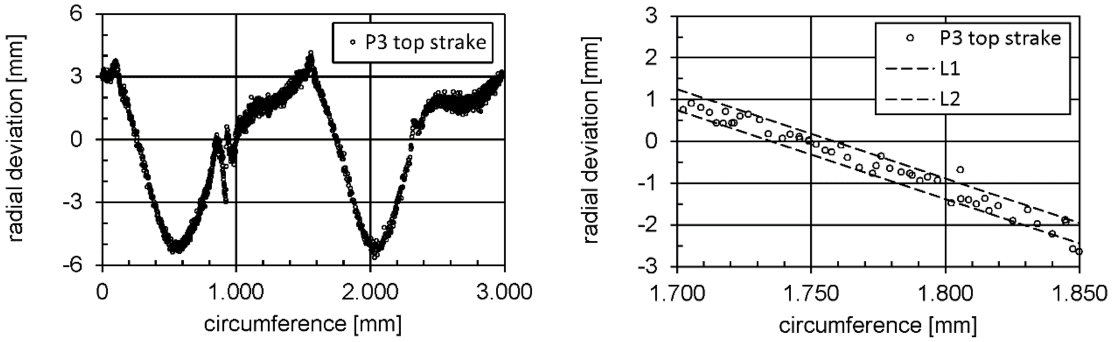

Fig. 3. Laser scan of example structure SX in chap. 4, plan view on radial deviations from a fitted perfect cylinder a) data from a horizontal slice of 5 mm height; b) detail with arbitrarily drawn bounding lines of 0,5 mm distance

From the data given in *Fig. 3* it can be concluded:

– Within a patch of 5 mm (meridional) x 50 mm (circumferential) there are app. 20 readings, which corresponds to a medium quadratic measuring grid of 3,5 mm.
– Apart from global out-of-roundness and other long-wave deviations, no localized or short-wave imperfections can be seen.
– Obviously, the scatter band of 0,5 mm width is representing rather the uncertainty of the measurement than real deviations of bumps in the shell wall. We assume, that the actual surface imperfection amplitude is smaller than ±0,15 mm which corresponds to ±T/20.
– In a stick measurement, this value would correspond to a bump depth of 0,3 mm or T/10, which is by far better than FTQC A, see Table **1**.
– Following hypothesis H5, our proposal is to use random imperfections within a range of ±T/20.
– Similar results have been found in (31) with measurements on wind turbine towers, where a 2 mm scatter band was associated with 30 mm wall thickness.

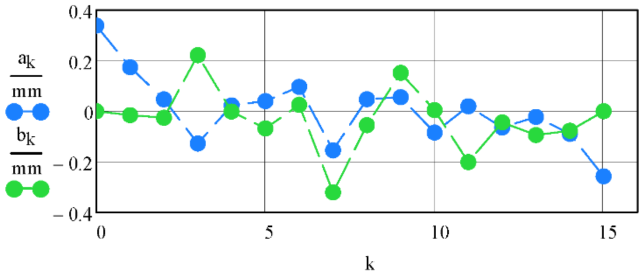

Fig. 4. Exemplary Fourier coefficients for row B, a set of 30 random numbers {–1 mm; +1 mm} note, that b_0 is per definition zero

Table 2. Exemplary Fourier coefficients for random numbers [mm] row B, see *Fig. 4*

Index	0	1	2	3	4	5	6	7	8
A	0,339	0,174	0,047	–0,128	0,023	0,040	0,096	–0,155	0,047
B	0	–0,016	–0,026	0,222	–0,001	–0,068	0,025	–0,321	–0,055
Index	9	10	11	12	13	14	15		
A	0,055	–0,085	0,020	–0,064	–0,023	-0,089	–0,258		
B	0,152	0,005	–0,202	–0,044	–0,094	–0,077	0		

The appropriate statistical model is termed *white noise*. In a very simple non-black-box procedure for the one-dimensional case, we generated 3 sets of random numbers by using an EXCEL feature (rows A, B and C). Each set had 30 values, so we could perform a DFT and determine 15 Fourier coefficients a (+ a_0) and b. Due to lack of space only row B is documented exemplary, see *Fig. 4* and Table 2.

A scheme for 2D random imperfections will be given in a future study. Imperfections for the panel itself are only needed with bolted tanks. In the present GMNIA examples we consider welded tanks, where the imperfections of the panels are dominated by the weld depressions. Thus, the panel imperfections don't need to be modelled.

5.4 Circumferential weld depression

The weld depression Type A developed in (6), (7) is a well established geometrical substitute imperfection for welded cylindrical structures under meridional compression. Due to the symmetry plane in the middle of the weld only cosine terms are needed for a Fourier representation. Due to the periodicity of the Fourier sum, equidistant welds can be described in one go.

The flanks of the weld depression have a fixed length, which is related to the bending half wave λ (see chap. 2). Thus, the Fourier coefficients, capturing the shape of the depression on one side and the periodicity on the other side, are depending on the ratio of the size of the depression and the length of the strake.

The Fourier coefficients can be determined by rigorous integration after inserting Eq. (8) in Eqs. (7). This leads to lengthy terms which are not documented here due to lack of space. Integration limits are from x = 0 (symmetry plane in weld) to x = $L_{strake}/2$ (symmetry plane in mid-strake). As can be seen from the examples given in chap. 4, the relation L_{dep}/L_{strake} ranges from 0,11 to 0,74 for typical dimensions.

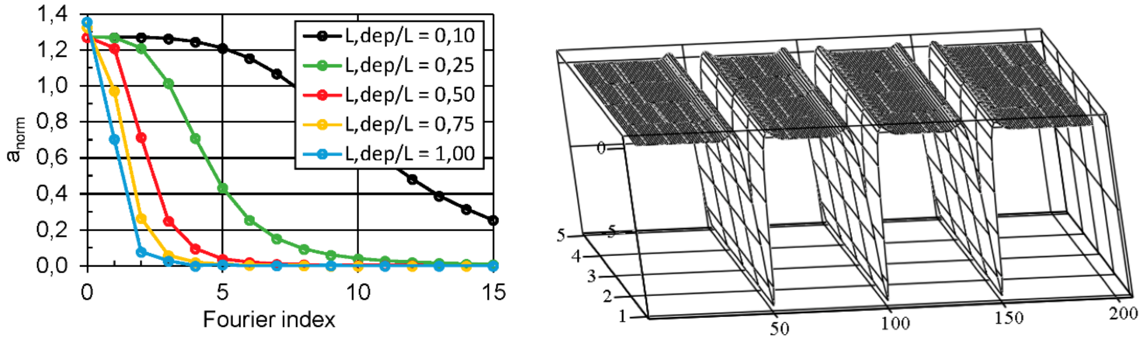

Fig. 5. a) Normalized Fourier coefficients a_{norm} for the weld depression Type A (6), (7), depending on the relation of L_{dep}/L_{strake}
b) Using one set of Fourier coefficients for equidistant dircumferential welds; the meridian is divided in 200 sections à 100 mm; the circumference is divided in quarters à 90°

$$a_{norm} = \frac{a \cdot L_{strake}}{w_0 \cdot \lambda} \tag{9}$$

A convenient way to normalize the coefficients a is given in Eq. (9). Typical results are given in Table 3 and *Fig. 5*.

Table 3. Normalized Fourier coefficients a_{norm} for the weld depression Type A (6), (7), depending on the relation of L_{dep}/L_{strake} , see *Fig. 5*

L_{dep}/L	0	1	2	3	4	5	6	7	8
0,25	1,273	1,269	1,213	1,018	0,711	0,434	0,254	0,151	0,093
0,50	1,273	1,211	0,717	0,250	0,096	0,038	0,021	0,010	0,007
0,75	1,328	0,974	0,265	0,057	0,020	0,008	0,004	0,002	0,001

5.5 Meridional weld depression

Information on longitudinal weld depressions will be given in a future study. The effect of imperfections is described in (32) and (33).

5.6 Localized bump

In many cases, the dominating pattern is a localized bump, see *Fig. 2*. When the bump is small compared to meridional length and/or circumference of the cylinder, coefficient matrices are needed, which might have more than 20 significant elements in each direction. An application example is given in chap. 6.3. We use Eq. (1) to describe the bump, because this gives a more pronounced information on where the bump ends compared to other bump functions found in literature.

5.7 Application rules

- Multiple, equidistant weld depressions along the meridian can be modelled by a single set of Fourier coefficients for the Rotter/Teng shape due to the inherent periodicity, as shown in 6.2 and *Fig. 6*.
- If the structure is made up of stepped wall-thickness, each of the circumferential welds should have a different amplitude. In this case it is recommended, to model each of the welds individually along a meridional range of $\pm L_{strake,i}$.
- A more complex imperfection pattern can be generated by adding up the coefficient matrices of the individual patterns.

$$[A_{m,n}]_{total} = [A_{m,n}]_{pattern\_1} + [A_{m,n}]_{pattern\_2} + \cdots \tag{10}$$

If more convenient, adding up can be done after generating the initial imperfections

$$[w_{m,n}]_{total} = [w_{m,n}]_{pattern\_1} + [w_{m,n}]_{pattern\_2} + \cdots \tag{11}$$

– If weld depressions and/or an excessive localized buckle is modelled, the plates in between may remain perfect.

5.8 Stainless steel and aluminium

Basically, the proposed generic imperfection patterns can be used with stainless steel structures and aluminium structures as well.

In EC3-1-6 (2) and EC9-1-5 (14) it is implied, that the imperfection sensitivity of stainless steel shells or of aluminium shells is identical or very similar to those of carbon structural steels, which can be seen from the design curves in the elastic regime. From a welding engineer's point of view, this is a very questionable assumption, because the range of welding parameters, heat input, thermal capacity and heat flux are really different (34).

6 EXEMPLARY GMNIA RESULTS FOR STEEL TANKS

6.1 Modelling and mesh size

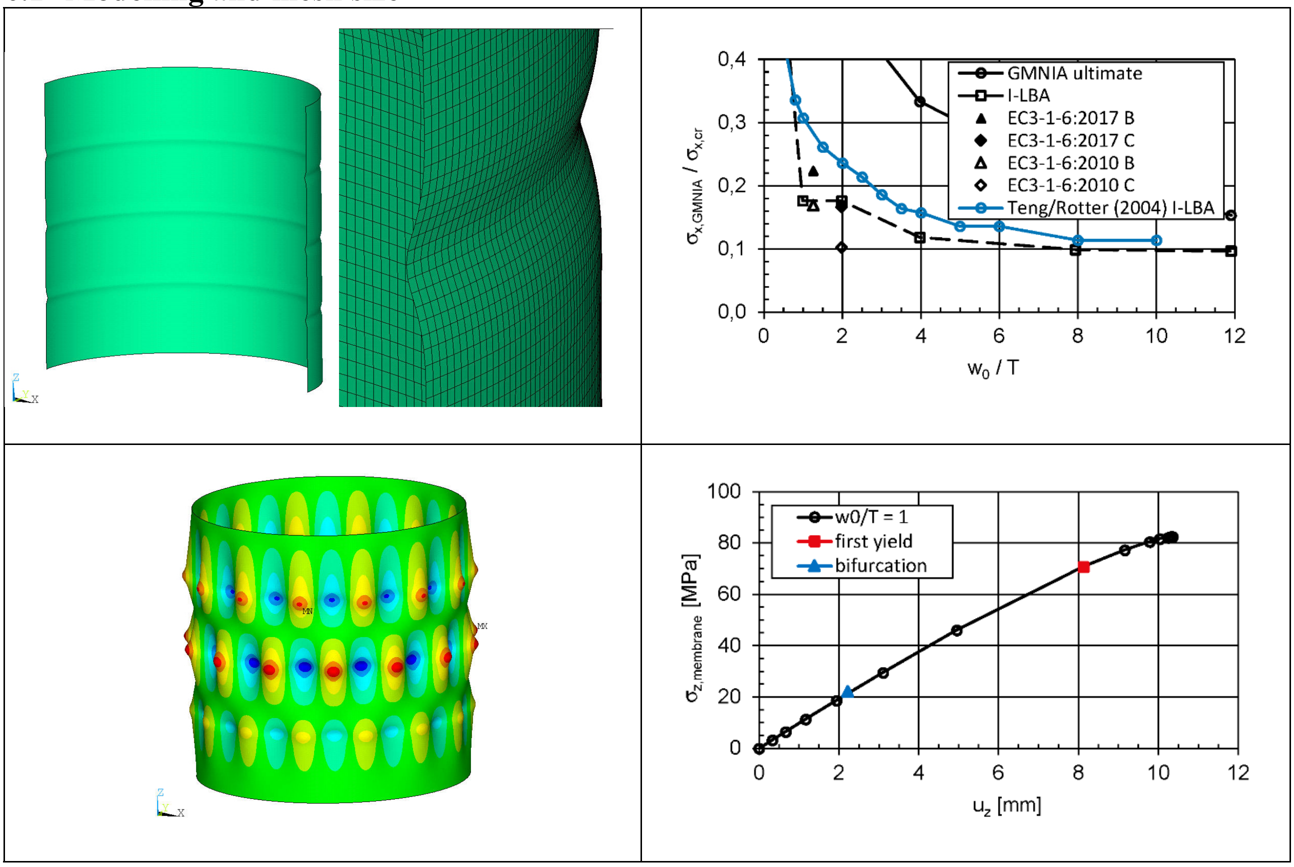

Fig. 6. a) Numerical simulation – Tank B with weld depressions and mesh
b) GMNIA/I-LBA results: imperfection sensitivity under axial compression
c) Eigenmode with w_0/T =2 and 14 circumferential waves
d) Merid. membr. stress vs. end shortening; non-convergence at 83 MPa; first yield at 71 MPa; bifurcation at 22 MPa

Specification of model and calculation procedure: ANSYS 20.2; global coordinates: X, Y are spanning the bottom plate, Z lies in the axis of revolution (right-hand rule); Shell 181 with full integration; units used are cm and kN; boundary conditions: bottom edge $u_{x,y,z} = 0$, top edge $u_{x,y} = 0$; loads are incremented by automated time-stepping, first step corresponds to $\Delta\sigma_x$ = 0,325 MPa resp. Δp = 0,56 kN/m²; modified Newton-Raphson scheme is used for equilibrium iterations;

6.2 Meridional compression with weld depression

Some exemplary GMNIA results for tank B (see chap. 4) are given in *Fig. 6*. For convenience, these are compared with the code provisions acc. to EC3-1-6 (2). Tank B has a relation L_{dep}/L_{strake} = 0,23. The Fourier coefficients have been determined according to chap. 5.4. Thus, the values are somewhat above the values given in Table 3 row 1. The imperfection sensitivity is in reasonable agreement with what should be expected acc. to (35), where the present results are conservative. This could be improved by a finer mesh at the weld depression.

6.3 Circumferential compression with localized bump

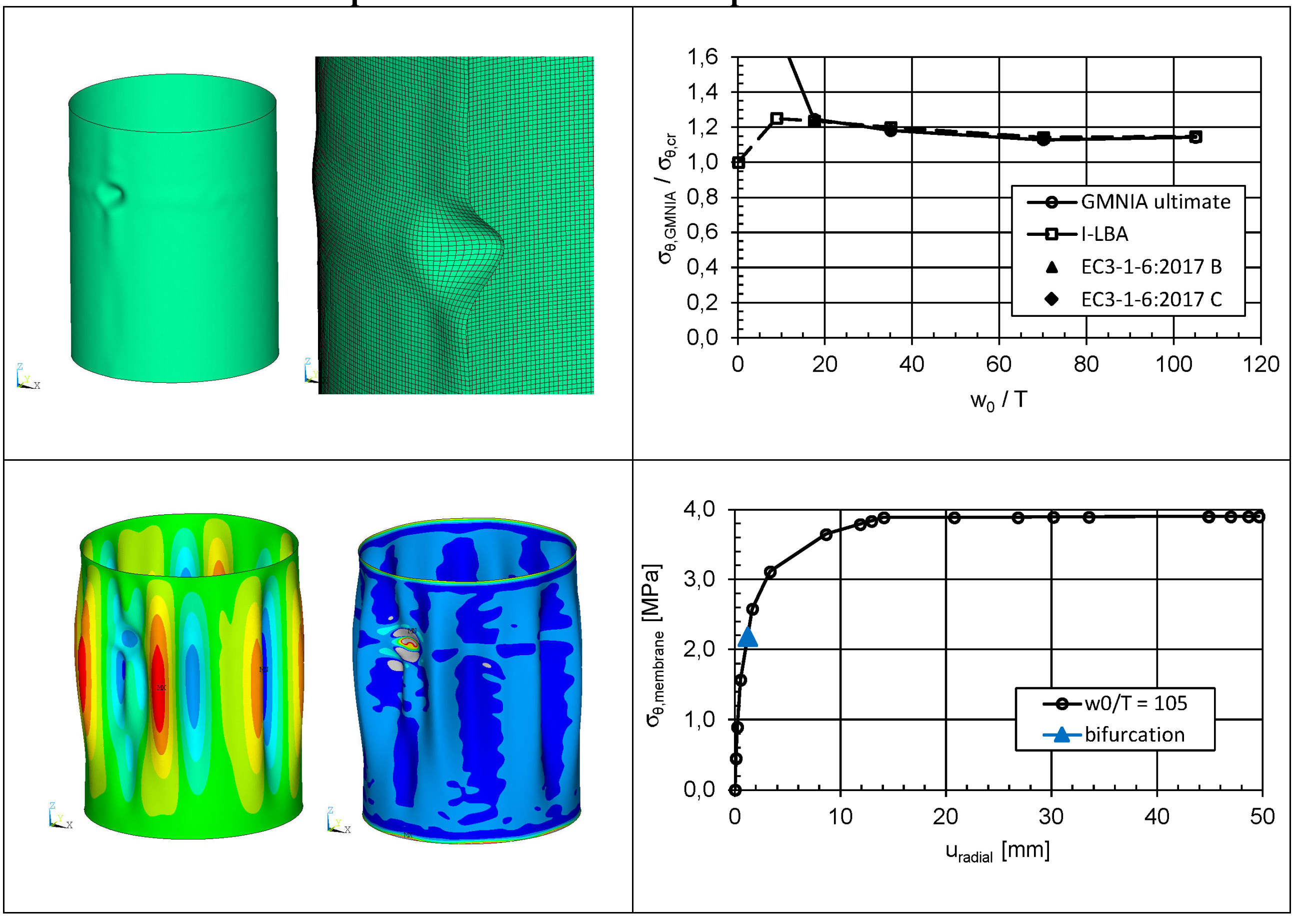

Fig. 7. a) Numerical simulation – Tank B (but D = 16 m) with localized bump at 0,7 L (d ≈ 1,70 m) and mesh
b) GMNIA/I-LBA results: imperfection sensitivity under external pressure
c) Eigenmode with w_0/T =2 and 14 circumferential waves
d) Merid. membr. stress vs. end shortening; non-convergence at 3,90 MPa; bifurcation at 2,19 MPa

7 OPEN QUESTIONS AND FURTHER RESEARCH

Although the proposed method seems to be quite promising in terms of simplifying the handling of imperfections in GMNIA, more work has to be done to confirm the hypotheses and assumptions given in 5.1 and gain more experience.

- The authors are currently having industry projects, where the proposed method will be applied. These projects will be the basis for extension of the proposed method.
- There is contradictory information in meridional weld depression: in (32), these depressions were investigated assuming the same depth as circumferential depressions, while in the recent measurements of (31) no significant meridional depressions were found.
- The influence of the size of a localized imperfection has not been investigated so far.
- By surveying a bolted tank, hypotheses H5 and H6 could be confirmed.

– Interaction of different types of imperfections with different load cases has not been investigated systematically so far. The circumferential weld depression, which is a severe imperfection for axial compression, is at the same time a ring stiffener with external pressure.

8 SUMMARY AND ACKNOWLEDGMENT

In the present study, the use of simplified imperfection patterns is proposed, which are represented by single or double Fourier series. This can facilitate the transfer of imperfections onto a numerical model, which is needed for GMNIA calculations. Examples for simplified patterns are given and the derivation of the respective Fourier coefficient matrices is shown.

The method is demonstrated with two application examples: a tank under axial compression with multiple weld depressions, and a tank with a localized bump under external pressure. Proposals for further research and for extending the method are given.

The authors are much obliged to Sergej Ponomarev, Matthias Hendriksen and Dr. Günter Fischbach from Ingenieurgesellschaft Dr.-Ing. Fischbach mbH, Erftstadt, Germany for providing an anonymized example tank (see *Fig. 2*).

Wolfgang Lang from P+W Metallbau GmbH & Co. KG, Meckenbeuren, Germany gave us permission to re-evaluate the data from the ZIM project (28), which is very much appreciated. The support of Marcel Mott from KIT Steel and Lightweight Structures is gratefully acknowledged. Marcel provided raw data from the ZIM project (28) and helped with the re-evaluation by means of CloudCompare.

REFERENCES

1. **Knödel, P. and Ummenhofer, T.** Regeln für die Berechnung von Behältern mit der FEM. *Stahlbau.* 2017, Vol. 86, 4, pp. 325-339.
2. **EN 1993.** *Design of steel structures. Part 1-6: Strength and stability of shell structures.* 2017.
3. **Knoedel, P.** Pitfalls in Shell Buckling FEA – Designers View. [ed.] M. Baeßler. *Proceedings, Buckling of Offshore Wind Energy Structures.* 2024.
4. **Bronstein, I. N. and Semendjajew, K. A.** *Taschenbuch der Mathematik.* Frankfurt : Harry Deutsch, 1974.
5. **EN 1090.** *Execution of steel structures and aluminium structures. Part 3: Technical requirements for aluminium structures.* 2019.
6. **Rotter, J.M. and Teng, J.G.** Elastic Stability of Cylindrical Shells with Weld Depressions. *Journal of Structural Engineering.* 5 1989, Vol. 115, pp. 1244-1263.
7. **Teng, J.G. and Rotter, J.M.** Buckling of Pressurised Axisymmetrical Imperfect Circular Cylinders Under Axial Loads. *ASCE Engineering Mechanics.* 2 1992, Vol. 118, pp. 229-247.
8. **Knoedel, P., Ummenhofer, T. and Rotter, J.M.** Rethinking imperfections in tanks and silos. [ed.] Ernst & Sohn. *ce/papers.* 2017, Vol. 1, No. 2 & 3, pp. 960-969.
9. **Rotter, J.M. and Schmidt, H., [ed.].** *ECCS TC8 TWG 8.4 Shells – Bucking of Steel Shells – European Design Recommendations, 5th Edition, 2008; Revised second imprint.* 2013.
10. **Bornscheuer, F.W., Häfner, L. and Ramm, E.** Zur Stabilität eines Kreiszylinders mit einer Rundschweißnaht unter Axialbelastung. *Stahlbau.* 1983, Vol. 52, pp. 313-318.
11. **Steinhardt, O. and Schulz, U.** Zum Beulverhalten von Kreiszylinderschalen. *Schweizerische Bauzeitung.* 1971, Vol. 89, 1, pp. 1-14.
12. **Li, Z., Pasternak, H. and Geißler, K.** Experiment-based statistical distribution of buckling loads of cylindrical shells. *Proc., Eurosteel, 12-14 September, Amsterdam, The Netherlands.* 2023, pp. 1816-1820.
13. **Mazzolani, F.M., Mandara, A., Di Lauro, G.** Buckling of Aluminium Shells: Proposal for European Curves. *4th Int. Conf. on Thin Walled Structures ICTWS 2004, 22-24 June 2004, Loughborough, U.K.* 2004.
14. **EN 1999.** *Design of aluminium structures. Part 1-5: Shell structures.* 2009.

15. **Knoedel, P. and Ummenhofer, T.** Practical Design of Aluminium Silos according to EC9-1-5. [ed.] F.M. Mazzolani and F. Bellucci. *13th International Aluminium Conference INALCO, September 21-23, Naples, Italy.* 2016, pp. 97-102.
16. **Radlbeck, C., et al.** Bemessung und Konstruktion von Aluminiumtragwerken. [ed.] U. Kuhlmann. *Stahlbaukalender.* 2016, pp. 175-309.
17. **Schmidt, H., Binder, B. and Lange, H.** Postbuckling strength design of open thin-walled cylindrical tanks under wind load. *Thin-Walled Structures.* 1988, Vol. 31, pp. 203-220.
18. **Rosin, J.** Stability of Steel Tanks with Unintentional Predeformation due to Installation. Structural safety analysis of a cylindrical steel tank with installation-induced large deformations using explicit FE analysis. *TÜV Süd Tagung Flachbodentanks International, München.* 2022.
19. **Ding, X., Coleman, R. and Rotter, J.M.** Technique for Precise Measurement of Large-Scale Silos and Tanks. *Journal of Surveying Engineering.* 1996, Vol. 122, 1, pp. 14-25.
20. **Soyk, G., Knödel, P. and Ponomarev, S.** Tankverstärkung ohne Schweißen – geklemmte Ringsteifen, Ertüchtigung im laufenden Betrieb. *TÜV Süd Tagung Flachbodentanks, Hamburg.* 2023.
21. **Ding, X., Colemann, R. and Rotter, J.M.** Surface Profiling System for Measurement of Engineering Structures. *Journal of Surveying Engineering.* 1996, Vol. 122, 1, pp. 3-13.
22. **Teng, J.G., et al.** Analysis of geometric imperfections in full-scale welded steel silos. *Engineering Structures.* 2005, Vol. 27, pp. 938-950.
23. **Sadowski, A.J., et al.** Harmonic analysis of measured initial geometric imperfections in large spiral welded carbon steel tubes. *Engineering Structures.* 2015, Vol. 85, pp. 234-248.
24. **Knoedel, P. and Ummenhofer, T.** Substitute Imperfections for the Prediction of Buckling Loads in Shell Design. [ed.] INSA. *Proc., Imperfections in Metal Silos – Measurement, Characterisation and Strength Analysis.* 1996, pp. 87-101.
25. **Stadtwerke Rostock.** Press release on a district heating tank in Rostock (in German), www.swrag.de/wir-fuer-hier/fuer-die-region/speicher, retrieved 01 Jan 2024 pk.
26. **Ummenhofer, T. and Knödel, P.** Behälterbau, master module lecture notes. Winter term 2023/2024 (unpublished). Karlsruhe : KIT Steel and Lightweight Structures, 2023.
27. **EN 485.** *Aluminium and aluminium alloys. Part 2: Mechanical properties.* 2016.
28. **Ummenhofer, T., et al.** Entwicklung neuartiger Konstruktionslösungen für materialeffiziente punktgestützte Metallsilobauerke auf Basis einer innovativen Berechnungsmethode. Abschlussbericht zum ZIM-Projekt, unveröffentlicht. [ed.] P+W Metallbau GmbH 88074 Meckenbeuren and KIT Steel and Lightweight Structures Karlsruhe. 2020.
29. **Hagenmeyer, C.** Experimental and numerical investigations on the load-bearing behaviour of locally supported aluminium silos under axial loading. Master thesis (in German) with Prof. Ummenhofer, Karlsruhe, KIT Steel and Lightweight Structures. 2019.
30. **EN 1993.** *Design of steel structures. Part 4-2: Tanks.* 2017.
31. **Kathirkamanathan, L., Sadowski, A.J. and Seidel, M.** Advanced structural analysis of digitally twinned metal wind turbine support towers. [ed.] M. Baeßler. *Proceedings, Buckling of Offshore Wind Energy Structures.* 2024.
32. **Hübner, A., Teng, J.G. and Saal, H.** Buckling behaviour of large steel cylinders with patterned welds. *International Journal of Pressure Vessels and Piping.* 2006, Vol. 83.
33. **Wunsch, C.** Study on the Numerical Shell Buckling Assessment (in German). Master thesis (in German) with Prof. Ummenhofer, Karlsruhe, KIT Steel and Lightweight Structures. 2016.
34. **Gkatzogiannis, S., Knoedel, P. and Ummenhofer, T.** Simulation of Welding Residual Stresses – from Theory to Practice. [ed.] C. Sommitsch, N. Enzinger and P. Mayr. *Mathematical Modelling of Weld Phenomena. Verlag d. Techn. Universität Graz.* 2018.
35. **Teng, J.G. and Rotter, J.M.** *Buckling of Thin Metal Shells.* London : Spon, 2004.